Hydrol. Earth Syst. Sci. Discuss., 9, 2797–2829, 2012
www.hydrol-earth-syst-sci-discuss.net/9/2797/2012/
doi:10.5194/hessd-9-2797-2012

Hydrology and Earth System Sciences Discussions

Hydraulic properties at the North Sea island Borkum derived from joint inversion of magnetic resonance and electrical resistivity soundings

T. Günther and M. Müller-Petke

Leibniz Institute for Applied Geophysics (LIAG), Stilleweg 2, 30655 Hannover, Germany

Received: 20 February 2012 – Accepted: 21 February 2012 – Published: 2 March 2012

Correspondence to: T. Günther (thomas.guenther@liag-hannover.de)

Published by Copernicus Publications on behalf of the European Geosciences Union.

Abstract

In order to do hydraulic modelling for simulating the salt-/fresh water dynamics, the parameters porosity, salinity and hydraulic conductivity are needed. We present a methodology retrieve them by the joint analysis of magnetic resonance (MRS) and and vertical electric (VES) soundings. Both data sets are jointly inverted for resistivity, water content and decay time using a block discretization.

We show the results of three soundings measured in the east part of the CLIWAT pilot area Borkum. Pumping test data is used to calibrate the petrophysical relationship for the local conditions. As a result we are able to predict porosity, salinity and hydraulic conductivities of the aquifers including their uncertainty.

The joint inversion significantly improves the reliability of the results, which can be shown by comparison with a borehole. By a sounding in the flooding area we demonstrate that only the combined inversion leads to a correct subsurface model. Thanks to the joint application we are able to distinguish fluid conductivity from lithology and provide reliable hydraulic parameters.

1 Introduction

The project CLIWAT (CLImate and groundWATer) investigates the impact of sea water rise on freshwater resources at the North Sea coast. One of the projects is specifically modelling the long-term hydraulic behaviour of the fresh water lens beneath the island of Borkum (Sulzbacher et al., 2012). Generally, for density driven flow models several input parameters are required such as porosity, hydraulic conductivity and salinity. Very often the needed quantities are not available at the catchment scale. By means of boreholes and direct investigations point information can be retrieved, however for large model these are usually not available sufficiently dense. Geophysics can play an important role to close the gaps between boreholes by one-dimensional soundings, two-dimensional or three-dimensional investigations. Airborne electromagnetic measurements are particularly important since they provide three-dimensional models of

HESSD
9, 2797–2829, 2012

resistivity (Siemon et al., 2009), which is a key parameter in hydrogeophysical investigations (Viezzoli et al., 2010). However, there are two main shortcomings of resistivity: (i) we cannot differentiate between clay content and fluid salinity and (ii) there is no sufficiently reliable relation to hydraulic conductivity, probably the most important parameter needed.

Geophysical techniques based on the principles of Nuclear Magnetic Resonance (NMR) can contribute to overcome these shortcomings. The method measures a signal arising from a set of hydrogen protons relaxing from an excited state back to equilibrium. This relaxation process can be described by exponentially decaying functions. NMR allows for uniquely determining water content of a sample based on the direct sensitivity on the number hydrogen proton represented by the initial amplitude of the exponential function. Furthermore, the measured decay time depends on the pore geometry and can therefore be used to estimate hydraulic permeabilities (Seevers, 1966). NMR is well known and established as laboratory and borehole method and with increasing success applied in the field scale. Surface NMR utilizes large surface loops to conduct electromagnetic pulses with increasing pulse moments q (product of current and duration), which successively reach deeper parts of the subsurface. For a detailed explanation of the surface NMR method see, e.g. Legchenko and Valla (2002); Hertrich (2008), particularly for parametrisation of hydrogeological systems see Lubczynski and Roy (2004); Lachassagne et al. (2005) and references therein.

An inversion retrieves water content and decay time in the subsurface as a function of depth. The most general approach was presented by Müller-Petke and Yaramanci (2010). They discretise the subsurface in the spatial (depth) and spectral (decay time) dimension and achieve a smooth image. However, very often the subsurface consists of distinct layers of constant properties, and a mono-exponential decay is a valid assumption for many unconsolidated sediments (Hertrich, 2008). Therefore we follow a block scheme that tries to invert for the parameters water content and decay time of a small number (typically 2 to 6) layers and their layer thicknesses. This approach is strictly using mono-exponential decay compared to the block scheme with stretched exponential decays presented by Behroozmand et al. (2011). We argue for the use of the simplest model that satisfies the data.

For calculation of surface NMR responses a resistivity model is needed that determines the magnetic fields in the subsurface (Weichman et al., 2000). Theoretically the resistivity could be retrieved from the measurements (Braun and Yaramanci, 2008). A simultaneous inversion for the three parameters, i.e. water content, decay time and resistivity, was done by Braun et al. (2009) using the time step inversion approach and a distinct number of layers with constant water content and mono-exponential decay times. However, the instruments do often not deliver reliable phases. Therefore, it is recommended to combine MRS with a direct current (DC), frequency domain electromagnetic (FDEM) or transient electromagnetic (TEM) sounding. For resistivity a block discretization is typical and can be solved by linear filtering and fast Hankel transformation (e.g. Anderson, 1989).

Since both methods are sensible to the typical structures of an aquifer system, a combined or joint inversion is favourable. The coupling of the methods is achieved only by the common layer thickness. Hertrich and Yaramanci (2002) presented a joint inversion scheme for resistivity and water content using a generalized Archie model yielding a differentiation between bound and mobile water. Our objective is to further include the decay times of NMR signals for both structural identification and hydrological characterisation.

There were a few papers dealing with retrieving hydraulic conductivity K from free induction decay (T_2^*) measurements in the field scale. For an overview see, e.g. Mohnke and Yaramanci (2008); Plata and Rubio (2008) and references therein. The relations go back to the model of Seevers (1966) using a second order dependence of K on the decay time T_2 and a first order dependence on the porosity Φ.

Close to our work, Vouillamoz et al. (2007) jointly interpret MRS and VES results and characterized aquifers based on NMR parameters and resistivity. The authors showed uncertainties of the derived parameters and demonstrated that inverting VES with fixed geometry from MRS significantly improved resistivity uncertainty.

In our paper we will present a methodology to invert for NMR parameters and resistivity simultaneously, the novel aspect being the QT block inversion applied for that. After briefly presenting the methodology we will present the results of three soundings measured in Borkum island. One of them is used for verification by comparing with a borehole. Another one is used for petrophysical calibration using a pumping test. Then we demonstrate on the third measurements how the three desired quantities are retrieved and how big the uncertainties are.

2 Methodology

2.1 MRS block QT modelling

We assume the resistivity model of the subsurface is known, e.g. from electric or resistivity soundings. The complex forward response (initial amplitudes) for a fixed discretisation can be formulated in terms of a matrix-vector multiplication

$$\tilde{\boldsymbol{u}} = \tilde{\mathbf{K}}\,\boldsymbol{f} \tag{1}$$

where $\tilde{\boldsymbol{u}}$ is the complex vector of simulated voltages, $\boldsymbol{w}$ is the searched water content vector and $\tilde{\mathbf{K}}$ is the complex-valued kernel. The latter depends on loop geometry and the resistivity distribution. Details about the computation can be obtained from Weichman et al. (2000) or Hertrich (2008). Usually instead of the complex data, amplitudes are inverted for by transforming Eq. (1) into a real-valued matrix-vector equation $\boldsymbol{u} = \mathbf{K}\,\boldsymbol{w}$. The problem becomes non-linear, i.e. $\mathbf{K}$ depends on $\boldsymbol{w}$. Since the kernel computation is extensive (calculation of B fields and integration from 3-D to 1-D), it is done only once for a relatively fine discretization. The forward response of an arbitrarily layer is then done by summing up all the original layers with their weight of coincidence between two models.

A QT type inversion (Müller-Petke and Yaramanci, 2010) means to use the whole data cube along both the pulse moment (q) and time (t) axis. Each value of the

HESSD

9, 2797–2829, 2012

Hydraulic properties on Borkum from joint MRS/VES inversion

T. Günther and M. Müller-Petke

response for a single layer, i.e. the amplitudes only from this layers, is then multiplied by the exponential function $e^{-t/T}$ forming the data cube. This is done for all layers and the values sum up. The latter function computes the forward response vector

$$\mathbf{f}(\mathbf{m}) = [E(q_1,t_1),...,E(q_1,t_T),E(q_2,t_1),...,E(q_Q,t_T)]^T$$

for given thickness values d_i, water contents θ_i and decay times T_i.

Even though the number of unknowns is very small ($3N$-1 where N is the number of layers), the number of data and thus the Jacobian matrix would become large due to the high sampling (typically 10 kHz) of the measured signals. Therefore we follow Behroozmand et al. (2011) and resample the individual decays into a number of about 40 gates using an integration procedure as known from TEM data processing. Logarithmically equidistant gates length are defined and the mean of all values within the gate is chosen. Thus, after gating the statistical error of a gate value changes from gate to gate as a function of the individual gate length. We calculate this error by dividing the error of data before gating by the square root of the number of values being averaged within a gate. This is equivalent to the usual stacking improvement assuming Gaussian distributed noise. Each individual gate error ϵ_i is then taken into account (cf. Eq. 2) using error weighted data inversion.

For the sake of clarity, the data error before gating is referred to as the noise level and can be obtained from (i) pure noise measurement or (ii) from imaginary part of the data after rotating (Müller-Petke et al., 2011). We decided for the latter since pure noise measurements were not available with the used instrument.

2.2 Inversion scheme

As typical for block inversion, we use a Marquardt-type damped Gauss-Newton inversion (Inman, 1975), i.e. using a local damping with successive cooling of the regularisation parameter. In order to account for the different measured quantities (ρ_a in Ωm and $E(t,q)$ in V) we apply a data weighting using independent errors ϵ_i for each datum

HESSD
9, 2797–2829, 2012

point. Hence, the data covariance matrix $\mathbf{C}_\mathrm{d}$ contains the variances ϵ_i^2 on the main diagonal. In each inversion step, the update $\Delta \boldsymbol{m}$ to the model m is retrieved by solving

$$\Delta \boldsymbol{m} = \left(\mathbf{J}^T \mathbf{C}_\mathrm{d}^{-1} \mathbf{J} + \lambda \mathbf{I}\right)^{-1} \mathbf{C}_\mathrm{d}^{-1} (\boldsymbol{d} - \boldsymbol{f}(\boldsymbol{m})), \tag{2}$$

where $\boldsymbol{f}$ denotes the forward operator, $\mathbf{J}$ is the Jacobian matrix and $\mathbf{I}$ is the identity matrix. The regularization parameter λ is successively decreased until convergence is reached. Since the number of unknowns is very small, a derivative of the forward response (the sensitivity matrix) is easily obtained by the perturbation method, i.e. a slight change of each individual value.

In inversion an improvement of result can be achieved by adding prior information about the valid parameter ranges. Therefore each of the unknowns p_i is transformed by a double-logarithmic transform (Kim et al., 1999; Günther, 2004) to the associated model parameter

$$m_i = \log(p_i - p_i^\mathrm{l}) - \log(p_i^\mathrm{u} - p_i) \tag{3}$$

with p_i^l and p_i^u being lower and upper bounds of p_i, respectively. The logarithmic transform has the advantage of automatically holding the values within bounds while decreasing the ill-posedness of the inverse problem. Table 1 gives an overview of the values used. They represent conservative bounds of values found in literature and could be further refined for each layer if prior knowledge is available.

The choice of starting models can be deciding since the algorithm can be trapped in local minima. In order to not driving the inversion too much, we use a homogeneous starting model of $\theta = 0.2$ and $T = 0.1$ s. For resistivity the mean of the apparent resistivity was used. Most deciding turned out to be the initial layer thickness. From the MRS kernel function we estimated a maximum depth comprising 80 % of the cumulative sensitivity (Christiansen and Auken, 2010) divided by the number of layers.

HESSD

9, 2797–2829, 2012

2.3 Joint MRS and VES inversion

A joint inversion is straightforwardly achieved by concatenating all data quantities, i.e. the combined response vector becomes $\boldsymbol{f} = [\boldsymbol{f}_{\text{MRS}}\ \boldsymbol{f}_{\text{VES}}]^T$. Hence the Jacobian matrix obtains the correct form of two concatenated matrices. Accordingly, the variance vector for building $\mathbf{C}_{\text{d}}$ is combined.

For a pure MRS inversion we must assume a resistivity distribution. To avoid biasing the result by using a contrasted resistivity model, we decided to use the Occam inversion result (Siemon et al., 2009) of the closest airborne EM sounding (cf. Fig. 1). The models are quite smooth and do not lead to provocation of layer boundaries. Whereas for the single MRS inversion this resistivity model remains constant, for a rigorous joint inversion we need to couple the improved VES result with the MRS using a kernel update. As a consequence, the joint model will change making an iterative approach necessary. Since a kernel update is expensive and to avoid the risk of being trapped in a local minimum, we update the resistivity in an outer loop. Experiments show that no more than 3 outer iterations, each fully minimizing the objective function, are needed.

Another important issue is the choice of the number of layers. In cases when no borehole is available, we suggest to start with a homogeneous case and increase the number of layers successively until no further decrease in the objective function is observed. Finally, appropriate initial values can guide inversion but also hinder convergence.

2.4 Computation of uncertainties

For a parameter estimation it is important to quantify the range in which the obtained values a expected to be. There are several ways of computing uncertainties, (i) based on the resolution matrix, (ii) based on the a-posteriori model covariance matrix, (iii) using most-squares inversion, and (iv) by a variation of individual parameters. As used by Müller-Petke et al. (2011), we decided for the latter way, i.e. varying the individual values independently unless the data confidence interval is exceeded. This method does not linearise and yields different values for lower and lower bound, that were however close to the values derived from the model covariance matrix. After successful inversion each parameter is varied until the forward response deviates from the solution by an amount associated to $\chi^2 = 1$. This corresponds in a statistical sense to a 95 % confidence interval.

Of course parameters are expected to infer each other. For example, the product water content and thickness of a layer denotes the amount of water being proportional to the signal strength and is better described than both parameters alone. However, in a hydrological investigation this corresponds to an aquifer test. Furthermore, the most influencing parameter, the decay time, is expected to be relatively independent on the other.

3 Experiments and results

3.1 Measurements and data processing

Target of the investigations was the eastern part of the separated fresh-water lens of Borkum, an area with dunes of significant topography. The latter restricted the layout of large loops needed for the targeted investigation depth of about 60 m. Four MRS soundings were acquired in spring 2010 in the frame of a BSc thesis (Liebau, 2010), where only amplitude were analysed.

Figure 1 shows the location of the measuring and reference loops along with VES positions, HEM flight lines and the borehole. One of the soundings, CL2, was placed in the middle of the dunes area describing the main extent of the fresh-water lens, close to a known research borehole (CLIWAT2) with known lithology for the validation of the method. Two other soundings, OD33 and P05, were conducted at the southern boundary of the dunes. They were situated at a water-well, where pumping tests have been carried out, with the aim of calibrating the hydraulic conductivity equation. The last one, SKD, was placed at the eastern boundary of the fresh-water lens, where a significant silt layer was presumed.

HESSD
9, 2797–2829, 2012

Magnetic field was about 49.3 µT and the corresponding Larmor frequency at about 2100 Hz. For all measurements, square loops with two turns (black rectangles) have been used in order to increase signal strength. The loop dimensions were chosen to reach the target depths after sensitivity analysis, i.e. about 50 m edge length in the center of the fresh-water lens and about 25 m in the flooding area where the investigation depth was restricted by salt water. We used the GMR instrument (Vista Clara Inc.), a multi-channel device with small instrument dead times. The pulse lengths for the first three soundings were 40 ms in order to maximize the pulse moment to about 7 As necessary for a deep penetration. For the smaller target depth of the fourth sounding we decreased the pulse length, which improves the ability of detecting fast decaying units such as silt (Dlugosch et al., 2011).

Additionally, reference loops have been laid out in order to capture the noise that can be removed from the signals using noise cancellation techniques (Müller-Petke and Yaramanci, 2011). Doing so, a major part of the present noise was already removed prior to further processing. The noise level of measurements is an important input parameter in inversion (cf. Eq. 2), particularly if different data types are combined. Overall a very good noise level was observed, decreasing from about 40 nV (CL2) over 20 nV (OD33/P05) down to 5 nV (SKD).

For the combined inversion the closest vertical electrical soundings have been picked out (see Fig. 1), having distances of not more than 50 m. The VES data have all been measured in the 1990ies and again in 2008. They comprise Schlumberger soundings with logarithmically increasing AB/2 starting from 1.5 m to about 150 m. Data quality was very good and the noise level was estimated with 3 % relative error. The latter is higher than the pure measurement error and includes electrode position errors and 3-D effects caused by small-scaled irregularities.

3.2 Sounding CL2: verification by borehole

The first sounding (CL2) was done directly at the research borehole CLIWAT 2, which was drilled in autumn 2009, six months before the MRS measurements. The borehole is located in the middle of the dune area where the fresh water lens reaches its maximum depth of more than 50 m. Lithology is well known from the interpretation of the drilling material. Furthermore, gamma ray and induction/resistivity log measurements have been carried out directly after the drilling to have a hint to clay content and lithology. Figure 2 shows the different available resistivity inversion alongside with the gamma log data and lithology interpretation.

On top there is a thick Holocene aquifer of clean fine sand with water table at about 3 m depth. It is followed by a silt-sand-clay layer surrounding the Holoceene base. Below 32 m there is a second, Pleistocene, aquifer of brown-gray fine sand followed by an inter-bedding of sand and clay at about 50 m. At that depth there is also the transition zone from fresh to salt water, which is clearly mapped by the vertical electrode chain (Grinat et al., 2010) or the array induction (AI) log. All three surface methods are generally able to detect the general course of resistivity but fail to yield a clear hint to lithology.

Resistivity variations in the fresh-water regime (100 Ωm or higher) do not significantly affect the kernel (Braun and Yaramanci, 2008). From the borehole we have a very good resistivity model that made a kernel-update obsolete. For joint inversion we chose a 5-layer model to account for the dry sand, the two aquifers, the aquitard and the conductive clay/salt-water zone where we do not expect an NMR signal.

In 11 iterations the total error-weighted misfit decreased to $\chi^2 = 1.15$. For both single and joint inversion a data fit of about 3 % could be obtained for the VES data, whereas the rms fit of MRS data was slightly below 40 nV. Data fit and the results of the joint inversion are shown in Fig. 3. The uppermost layer is the unsaturated zone characterized by high resistivity and low water content. Otherwise the water content variations are in total very small (21–31 %).

The first aquifer is characterized by resistivities of about 100 Ωm, 30 % water content and 200 ms decay time, which is relatively high for fine sand (Schirov et al., 1991; Lubczynski and Roy, 2003). Since the MRS measured T_2^* decay time is, besides the sensitivity to pore sizes, influenced by magnetic gradients, either at the pore or globally,

HESSD
9, 2797–2829, 2012

this decay time indicates sand with low amounts of magnetic impurities or iron oxides at the grain surface. The first aquitard is imaged at the correct position as conductive layer with less water content and decreased decay time, but the thickness appears too small. The second aquifer exhibits increased resistivity compared to the aquitard but still lower resistivity compared to the first aquifer and a slightly lower water content. The latter might be explained by either a higher degree of compaction or a compensation effect due to a too large thickness.

Remarkably, the decay time of the second fine sand aquifer is far lower than for the first even though the amount of small grains is very small according to the borehole description and not significantly different. Smaller decay times may be caused by magnetic gradients at pore scale due to magnetic impurities or iron oxides at the grain surface or in the fluid. Grunewald and Knight (2011) showed this influence as decreasing T_2^* with increasing magnetic susceptibility of the grains. From borehole logs we observed an increased susceptibility in the second aquifer. This is partly supported by the brownish color, but cannot be proved without samples. Nevertheless, since the genesis of this layer is different from the primary aquifer internal pore scale gradients due to magnetic impurities only in the second aquifer are possible. The sensitivity of the MRS measured T_2^* decay time to magnetic gradients is a disadvantage compared to laboratory T_2 decay times. Measuring T_1, the longitudinal relaxation (Legchenko et al., 2004), avoids the ambiguity. Recently Walbrecker et al. (2011) presented a new scheme to reliably estimate T_1 from MRS measurements.

The above comparison of water content, decay time and resistivity with ground truth shows a main advantage of combined application of MRS and VES. Both T_2^* decay times and resistivity interpreted solitary are ambiguous. Fast decay may be due to smaller pores or magnetic gradients. Low resistivity may be salt water pore fluid or clay content. However, low resistivity with high decay times uniquely indicates an effect due to salt water, whereas small decay times with high resistivity indicate magnetic gradients.

Before the obtained quantities can be further used, we are interested in their accuracy. As described above, we vary each model parameter individually until the model response leaves the error model around the response from the best model. The range of valid models is expressed by the error bars (see Fig. 3), which are relatively large for water content. The variation of the decay time is far lower and increases with depth, nevertheless the different units are significantly different. The best parameter is resistivity, which is resolved in tight bounds.

Generally the NMR parameters are poorly determined for the unsaturated zone due to the small signal. Also the thin aquitard has a bad resolution and can not significantly be distinguished from the neighbouring layers. The thickness values have a quite good uncertainty because here all three parameters combine their resolution. Only the last layer boundary is not well defined due to the high conductivity. In total, the uncertainty analysis shows that for this medium quality data as in this case a quantitative analysis needs to be done with caution.

3.3 Soundings OD33: hydraulic calibration

The next two soundings are located at the southern boundary of the dunes, where the thickness of the fresh-water layer is significantly reduced. We used the identical experimental setup (cf. Table 2). Since the results are very similar, we show only OD33, a sounding that was made next to a well where pumping tests have been carried out (Sulzbacher et al., 2012). We decided for a four-layer case, because a five-layer case did not significantly reduce the data fit. Data fit and results are shown in Fig. 4.

Due to the small distance to CL2 the lithology is expected to be similar. Accordingly, the first aquifer with almost identical properties (≈31 % porosity, 200 ms decay time and about 80 Ωm resistivity). Below, there is also a shallow, conductive layer with decreased decay time, which is therefore interpreted as silt. In contrast to CL2, the decay times of the second aquifer show again values of about 200 ms instead of 70 ms. Even though the resistivity indicates fresh water in this layer, historically this layer is presumed to been salt water saturated before the modern embankments were created

HESSD
9, 2797–2829, 2012

(Sulzbacher et al., 2012). We suspect that the aggressive fluid in the salt water region has washed out the iron from the fluid or the grain surface in the past.

Looking at the uncertainties the overall parameter resolution is significantly better than for CL2. Exceptions are the NMR parameters of the unsaturated zone and the silt layer. Also, the upper boundary of the silt is fairly uncertain, whereas its thickness is much better determined. While the models at CL2 underestimated the thickness is this first aquitard at OD33 the position and thickness agrees better with the borehole information. Due to the improved (by a factor of two) MRS data quality and the large contrast in the decay times the silt layer can be nicely inverted and supports the improved resistivity inversion by the joint inversion.

3.4 Sounding SKD: complex salt-water dynamics

The last sounding was done at the easternmost boundary of the fresh-water lens close to the North Sea. In this flat area storm surges, as known from the storm Kyrill in 2007, are regularly adding salt-water from top. In this vulnerable zone between deep salt-water intrusion and surface salinity the dynamics depends highly on the distribution of the hydraulic conductivity. We used a smaller loop (25 × 25 m), shorter pulses and a higher number of pulse moments, resulting in a higher resolution for the shallow depths. The data quality was very excellent, after rotation about 4–5 nV noise remained in the imaginary part.

For the VES measurement there was no measurement in the direct vicinity (cf. Fig. 1). However by comparing two soundings at the same distance to the dunes we found only little differences which hints to 2-D conditions. Therefore we are confident with the closest measurement for the joint inversion, about 150 m south from the MRS coil. From neighbouring boreholes a shallow and thick silt layer was presumed, but we had no reliable idea of the subsurface layering. Therefore we first conducted independent inversions of both data sets and increased the number of layers subsequently. The MRS data could already be fitted to a χ^2 level of 1.2 using a three-layer case (see Fig. 5a, b).

HESSD
9, 2797–2829, 2012

Whereas water content is almost constant about 30 %, the decay times showed a significant decrease from 200 to 75 ms in the second layer, which can be interpreted as the silt layer. On the other hand, four layers were needed to fit the VES data, which is obvious from the apparent resistivity curve (Fig. 5f). The values itself are very low hinting to large salt concentrations in the fluid. An interpretation of the resistivity model alone is however hard since silty or clayey layers have similar resistivity as salt or brackish water in sand.

The position of the second layer boundary is amazingly equal, which gives hope for a successful joint inversion. Again we tried with small layer numbers but a significant decrease of the fit close to the error level was only possible with 5 layers ($\chi^2 = 1.07$), as already the independent results indicate. Figure 6 shows the joint inversion result. The model responses can hardly be distinguished from the single inversions. The models are generally similar but significantly different.

On top is again a sandy layer (200 ms decay time) with already low resistivity originating from the flooding. The good conductor below is, as in Fig. 5, split into two different decay times, most probably a sandy layer with 200 ms and a silt layer of 75 ms. The silt obtains slightly higher water content, which is very plausible, although the uncertainties are bigger than the overall variations. The uncertainties of the second and third layer point out that they cannot be distinguished with resistivity methods, but well by the T_2^* time.

Below this silt layer there is fine sand again with large decay times, but a resistivity jump from about 20 down to 2 Ωm. We interpret the upper as laterally influenced by the fresh water lens, which is much shallower as in the dunes and more conductive due to lateral diffusion of salt water. Looking at the uncertainties we see that the best determined parameter is the decay time, followed by resistivity. Water content, although nicely detected by MRS, cannot be used for discrimination. The uncertainties of the layer thicknesses increase with depth, but are very small due to the fact that all three parameters contribute to it. In total the model can be considered very reliable even if no ground truth can be used. Several facts are responsible for it: the very low absolute

HESSD
9, 2797–2829, 2012

noise level and the large amount of stacks, the number of pulse moments and the short dead time that makes a clear detection of fast-decaying water possible.

4 Hydraulic properties and uncertainty analysis

4.1 Derivation of hydraulic properties

The long-term hydraulic modelling (Sulzbacher et al., 2012) needs the distribution of the following input parameters: porosity, current salt concentration and hydraulic conductivity. All three obtained parameters can be derived from the quantities obtained in the joint inversion.

Porosity equals the NMR water content in the case of full saturation. However, the latter must be interpreted as mobile water, adhesive water in very small pores probably lead to a underestimation of the total porosity if clayey material is present (Lubczynski and Roy, 2005). Vouillamoz et al. (2007) introduced an additional calibration factor for MRS water content to total porosity. This calibration is derived from pumping tests via specific yield in the case of unconfined sandy aquifer. We do not expect large amounts of clayey material and thus we forbear calculating another calibration factor.

Salt concentration is deduced from a modified Archie equation, relating fluid conductivity σ_{bf} and bulk conductivity σ_b:

$$\sigma_b = \sigma_f \cdot F + \sigma_s = \sigma_f \Phi^{-m} + \sigma_s, \quad (4)$$

where σ_s is a surface conductivity originated from fine material and F is the formation factor, which is related to porosity by the cementation factor m. Even though there are widely used literature values σ_s and m can be obtained on-site.

Therefore, the data of about 15 direct push soundings in the survey area were used that measured both bulk resistivity by a four-point measurement and took fluid samples for retrieving fluid conductivity. We used 25 data pairs from the first aquifer in a wide range of salt concentrations and fitted a curve through it with the result of $\sigma_s = 3.66e$-$3\,\mathrm{S\,m^{-1}}$ and $F = 0.2612$. From the obtained porosity of the first aquifer the latter is equivalent to a cementation exponent of m=1.26, very close to literature values of 1.3 for loose sand. These values are subsequently used to derive the fluid conductivity from porosity ϕ and resistivity ρ and further deduce a NaCl concentration. This procedure is in contrast to Vouillamoz et al. (2007) who used a rough linear equation with a single calibration factor to estimate the conductivity of the pore fluid from bulk conductivity due to expected clay contents that prohibit the use of Archie.

Hydraulic conductivity K is obtained from porosity ϕ and decay time T_2^* using a semi-empiric equation after Kenyon (1997)

$$K = c\Phi^a T_2^b \tag{5}$$

with a, b, c being site-specific calibration factors including fluid flow relevant parameters such as cementation and tortuosity but also NMR rock parameter such as surface relaxivity. We use an early proposed set of factors from Seevers (1966),

$$K = C_k \Phi T_2^2, \tag{6}$$

validated on quartz powder and sandstones (small porosities), both measured in laboratory conditions (T_2 instead of T_2^*). However, C_k still needs a calibration. Several authors have used this equation and observed appropriate values for C_K between $30e$-4 and $326e$-$4\,\mathrm{m\,s^{-3}}$ (Mohnke and Yaramanci, 2008).

Except grain size analyses or flow experiments, a standard method in the aquifer scale is to carry out pumping tests. Several of these were conducted in the east of Borkum in water test wells. Additionally, fluid conductivities are well-known. We chose the well OD33 for calibration since there is a simple situation with a typical fine sand aquifer that is far away from pumping wells.

For the upper aquifer of OD33, a transmissivity of $9.86\,\mathrm{m^2\,s^{-1}}$ was determined from a pumping test (Sulzbacher et al., 2012). Taking the determined thickness of 14 m into account, this corresponds to a hydraulic conductivity of $K = 7.04e$-$5\,\mathrm{m\,s^{-1}}$. By insertion

HESSD
9, 2797–2829, 2012

the porosity $\phi = 32.3\,\%$ and decay time $T_2 = 215\,\text{ms}$ into Eq. (6) we obtain a calibration factor of $C_S = 47e\text{-}4\,\text{m}\,\text{s}^{-3}$, well within the literature ranges.

Since OD33 was used for calibration of hydraulic conductivity, CLIWAT2 exhibits a poorer data quality, we show the derivation of the hydraulic parameters for the sounding SKD. As described, each two of the three primary parameters are combined to obtain hydraulic conductivity and fluid conductivity, expressed as total dissolved solids (TDS) using a Chloride (Cl^-) concentration conversion factor derived by Sulzbacher et al. (2012) from water sample analyses. We did not apply the Archie equation for the silt layer since we do not know its surface conductivity. The results are summarized in Table 3.

The hydraulic conductivities of the fine sand layers are in a very plausible range between $4e\text{-}5$ and $7e\text{-}5\,\text{m}\,\text{s}^{-1}$. Only the last layer exhibits an high value due to the unusually high T_2^*.

The TDS concentrations of the lowest layer are close to that of sea water. The same holds for the second layer, where salt water inserted by flooding events is obviously assembling on top of the silt, which is acting as a semi-permeable barrier. Both the top layer and the layer beneath the silt show brackish conditions.

4.2 Uncertainty of the derived parameters

As the primary results of any physical experiment require a measure of reliability or uncertainty, the final outcome of our survey requires uncertainties of the determined hydraulic parameters ϕ, K and TDS. We apply the rules of error propagation, i.e. the errors of all parameters add up to the error of the target value.

The retrieved TDS concentrations obtain the same relative error as the fluid conductivity or resistivity. Furthermore we assume cementation exponent and surface conductivity being constant. The first should not vary that much and the latter plays only a minor role in sandy sediments. From Eq. (4) we can directly derive using rules of error propagation,

HESSD
9, 2797–2829, 2012

Hydraulic properties on Borkum from joint MRS/VES inversion

T. Günther and M. Müller-Petke

$$\frac{\delta \mathrm{TDS}}{\mathrm{TDS}} = \frac{\delta \sigma_f}{\sigma_f} = \frac{\delta \sigma_\mathrm{b}}{\sigma_\mathrm{b} - \sigma_\mathrm{s}} + m \frac{\delta \Phi}{\Phi} \quad (7)$$

As a first order approximation, the relative error is slightly higher than the sum of the relative errors of both primary parameters. Similarly, we derive from Eq. (6)

$$\frac{\delta K}{K} = \frac{\delta C_S}{C_S} + \frac{\delta \Phi}{\Phi} + 2\frac{\delta T_2^*}{T_2^*} \quad (8)$$

Of course the parameters are not completely independent, e.g. an overestimation of water content is often accompanied by an underestimation of decay time. However we can use the result as a conservative guess. The first factor can only be retrieved from the calibration itself and is of the same order of the rest (relative error in porosity and twice the relative error in decay time). If several calibration wells are available, the uncertainty in C_S can be drastically decreased and additionally be estimated from the variation of the retrieved values.

We apply Eqs. (7) and (8) to the results of SKD and assume the calibration factor known in order to show what we can achieve in case of a good sounding. The relative deviations of all parameters are summarized in Table 4.

The relative primary parameter variations are all between half an order of magnitude, most of them at about 10–20 %. Worst values are obtained for the silt and the lower-most layer, where the resolution is low. Consequently, for these also the secondary parameters are not well resolved. However, the three sandy layers show very small ranges due to the good data quality.

Overall, Vouillamoz et al. (2007) presented slightly but generally higher uncertainties. There are some reasons for this. (i) As shown by Vouillamoz et al. (2007) including a fixed geometry, here derived from MRS, decreases uncertainty. Our joint inversion of MRS and VES combines the best of both methods and improves resolution and therefore decreases uncertainties. (ii) QT inversion as shown by Müller-Petke and Yaramanci (2010) is a more general and accurate approach. The block-QT inversion reduces the number unknown and therefore the accuracy of its estimation. (iii) Noise

Cancellation techniques improved the data quality of MRS significantly. The data presented have very good S/N ratio. (iv) Vouillamoz et al. (2007) calculated the uncertainty from statistics of many field MRS and VES measurements in contrast to the uncertainty analysis of a single excellent data quality sounding.

5 Conclusions and outlook

We presented a new scheme inverting the whole data cube (QT type) of magnetic resonance sounding in terms of block models of water content and mono-exponential decay time. This block-QT inversion is furthermore extended to a joint inversion with resistivity data. The combination is done straightforwardly by coinciding layer thickness values. In addition, the resistivity obtained is included into MRS forward calculation.

For the presented study area of salt-/fresh water interference the joint MRS and VES inversion yields superior results compared to single inversions. While interpretation of resistivity or decay time alone is ambiguous, a joint application and interpretation allows for differentiating lithology and salinity. A change in salinity affects resistivity but not decay time, and a change in lithology affects resistivity and decay time. The combination provides all parameters needed for hydraulic modelling, i.e. porosity, hydraulic conductivity and salinity together with uncertainty values if the petrophysical relations can be assumed and calibrated. Nevertheless, a validation and calibration with boreholes, pumping tests, direct push etc., will always be necessary. Very easily the DC resistivity data could be replaced by frequency EM (ground or airborne) or transient TEM soundings or a combination of them.

If the subsurface is not strictly layered, a two- or three-dimensional QT imaging is needed. However, for a 3-D characterization at the catchment scale only point NMR information can be efficiently retrieved. Since Airborne electromagnetic is efficiently used to retrieve 3-D resistivity models, statistical methods could fill the gap for finally obtaining three-dimensional hydraulic models, which would be needed for a holistic understanding of aquifer systems and finally to appraise the impact of climate change on groundwater systems.

HESSD
9, 2797–2829, 2012

Acknowledgements. We like to thank Robert Meyer and Jobst Liebau for acquiring the field data. We are grateful for valuable hints from Franz Binot concerning the geology and Thomas Wonik for providing borehole data. Furthermore we like to acknowledge the authors of the MRSMatlab toolbox for providing their codes for data processing and kernel calculation.

References

Anderson, W.: A hybrid fast Hankel transform algorithm for electromagnetic modeling, Geophysics, 54, 263–266, 1989. 2800

Behroozmand, A., Auken, E., Fiandaca, G., Dalgaard, E., and Larsen, J.: Full FID Inversion of MRS Data, in: Ext. Abstr. 17th Eur. Meeting of Environm. and Engineering Geophysics, 2011. 2800, 2802

Braun, M. and Yaramanci, U.: Inversion of resistivity in Magnetic Resonance Sounding, J. Appl. Geophys., 66, 151–164, doi:10.1016/j.jappgeo.2007.12.004, 2008. 2800, 2807

Braun, M., Kamm, J., and Yaramanci, U.: Simultaneous inversion of magnetic resonance sounding in terms of water content, resistivity and decay times, Near Surf. Geophys., 7, 589–598, doi:10.3997/1873-0604.2009010, 2009. 2800

Christiansen, A. V. and Auken, E.: A global measure for depth of investigation in EM and DC modeling, in: Ext. Abstr. 21th Int. Geophys. Conf. of the Aust. Soc. Explor. Geophys, Sydney, Australia, 2010. 2803

Dlugosch, R., Müller-Petke, M., Costabel, S., Günther, T., and Yaramanci, U.: Assessment of the potential of a new generation of surface NMR instruments, Near Surf. Geophys., 9, 89–102, 2011. 2806, 2821

Grinat, M., Südekum, W., Epping, D., Grelle, T., and Meyer, R.: An Automated Electrical Resistivity Tomography System to Monitor the Freshwater/saltwater Zone on a North Sea Island, in: Ext. Abstr. 14th Eur. Meeting of Environm. and Engineering Geophysics, 2010. 2807

Grunewald, E. and Knight, R.: The effect of pore size and magnetic susceptibility on the surface NMR relaxation parameter T_2^*, Near Surf. Geophys., 9, 169–178, doi:10.3997/1873-0604.2010062, 2011. 2808

Günther, T.: Inversion Methods and Resolution Analysis for the 2D/3D Reconstruction of Resistivity Structures from DC Measurements, Ph.D. thesis, University of Mining and Technology Freiberg, available at: http://nbn-resolving.de/urn:nbn:de:swb:105-4152277, 2004. 2803

HESSD

9, 2797–2829, 2012

Hydraulic properties on Borkum from joint MRS/VES inversion

T. Günther and M. Müller-Petke

Hertrich, M.: Imaging of groundwater with nuclear magnetic resonance, Prog. Nucl. Mag. Res. Sp., 53, 227–248, doi:10.1016/j.pnmrs.2008.01.002, 2008. 2799, 2801

Hertrich, M. and Yaramanci, U.: Joint inversion of Surface Nuclear Magnetic Resonance and Vertical Electrical Sounding, J. Appl. Geophys., 50, 179–191, 2002. 2800

Inman, J. R.: Resistivity inversion with ridge regression, Geophysics, 40, 798–917, 1975. 2802

Kenyon, W. E.: Petrophysical Principles of Applications of NMR Logging, The Log Analyst, 38, 21–43, 1997. 2813

Kim, H., Song, Y., and Lee, K.: Inequality constraint in least-squared inversion of geophysical data, Earth Planets Space, 51, 255–259, doi:10.1088/1742-2132/8/1/004, 1999. 2803

Lachassagne, P., Baltassat, J., Legchenko, A., and de Gramot, H. M.: The links between MRS parameters and the hydrogeological parameters, Near Surf. Geophys., 3, 259–266, doi:10.3997/1873-0604.2005021, 2005. 2799

Legchenko, A. and Valla, P.: A review of the basic principles for proton magnetic resonance sounding measurements, J. Appl. Geophys., 50, 3–19, doi:10.1016/S0926-9851(02)00127-1, 2002. 2799

Legchenko, A., Baltassat, J.-M., Bobachev, A., Martin, C., Robain, H., and Vouillamoz, J.-M.: Magnetic Resonance Sounding Applied to Aquifer Characterization, Ground Water, 42, 363–373, doi:10.1111/j.1745-6584.2004.tb02684.x, 2004. 2808

Liebau, J.: SNMR measurements in the east of Borkum, BSc thesis, University of Leipzig, 2010. 2805

Lubczynski, M. and Roy, J.: Hydrogeological interpretation and potential of the new magnetic resonance sounding (MRS) method, J. Hydrol., 283, 19–40, doi:10.1016/S0022-1694(03)00170-7, 2003. 2807

Lubczynski, M. and Roy, J.: Magnetic Resonance Sounding: New Method for Ground Water Assessment, Ground Water, 42, 291–309, doi:10.1111/j.1745-6584.2004.tb02675.x, 2004. 2799

Lubczynski, M. W. and Roy, J.: MRS contribution to hydrogeological system parametrization, Near Surf. Geophys., 3, 131–139, doi:10.3997/1873-0604.2005009, 2005. 2812

Mohnke, O. and Yaramanci, U.: Pore size distributions and hydraulic conductivities of rocks derived from Magnetic Resonance Sounding relaxation data using multi-exponential decay time inversion, J. Appl. Geophys., 66, 73–81, doi:10.1016/j.jappgeo.2008.05.002, 2008. 2800, 2813

Müller-Petke, M. and Yaramanci, U.: QT-Inversion – Comprehensive use of the complete surface-NMR dataset, Geophysics, 75, WA199–WA209, doi:10.1190/1.3471523, 2010. 2799, 2801, 2815

Müller-Petke, M. and Yaramanci, U.: Noise Cancellation for surface NMR: Derivation of time and frequency domain approaches, in: Ext. Abstr. 17th European Meeting of Environmental and Engineering Geophysics, Leicester, UK, 2011. 2806

Müller-Petke, M., Dlugosch, R., and Yaramanci, U.: Evaluation of surface nuclear magnetic resonance-estimated subsurface water content, New J. Phys., 13, 095002, doi:10.1088/1367-2630/13/9/095002, 2011. 2802, 2804

Plata, J. L. and Rubio, F. M.: The use of MRS in the determination of hydraulic transmissivity: The case of alluvial aquifers, J. Appl. Geophys., 66, 128–139, 2008. 2800

Schirov, M. D., Legchenko, A., and Creer, G.: A new direct non-invasive groundwater detection technology for Australia, Explor. Geophys., 22, 333–338, doi:10.1071/EG991333, 1991. 2807

Seevers, D.: A nuclear magnetic method for determining the permeability of sandstones, Society of Professional Well Log Analysts Transactions, Paper L, 14 pp., 1966. 2799, 2800, 2813

Siemon, B., Christiansen, A., and Auken, E.: A review of helicopter-borne electromagnetic methods for groundwater exploration, Near Surf. Geophys., 7, 629–646, 2009. 2799, 2804

Sulzbacher, H., Wiederhold, H., Siemon, B., Grinat, M., Igel, J., Burschil, T., Günther, T., and Hinsby, K.: A modelling study of the freshwater lens of the North Sea Island of Borkum, Hydrol. Earth Syst. Sci. Discuss., in press, 2012. 2798, 2809, 2810, 2812, 2813, 2814

Viezzoli, A., Tosi, L., Teatini, P., and Silvestri, S.: Surface water-groundwater exchange in transitional coastal environments by airborne electromagnetics: The Venice Lagoon example, Geophys. Res. Lett., 37, L01402, doi:10.1029/2009GL041572, 2010. 2799

Vouillamoz, J., Chatenoux, B., Mathieu, F., Baltassat, J., and Legchenko, A.: Efficiency of joint use of MRS and VES to characterize coastal aquifer in Myanmar, J. Appl. Geophys., 61, 142–154, doi:10.1016/j.jappgeo.2006.06.003, 2007. 2800, 2812, 2813, 2815, 2816

Walbrecker, J. O., Hertrich, M., Lehmann-Horn, J. A., and Green, A. G.: Estimating the longitudinal relaxation time T1 in surface NMR, Geophysics, 76, F111–F122, doi:10.1190/1.3549642, 2011. 2808

Weichman, P. B., Lavely, E. M., and Ritzwoller, M. H.: Theory of surface nuclear magnetic resonance with applications to geophysical imaging problems, Phys. Rev. E, 62, 1290–1312, doi:10.1103/PhysRevE.62.1290, 2000. 2800, 2801

HESSD

9, 2797–2829, 2012

Table 1. Lower and upper parameter bounds for the individual parameters.

Parameter	p	p^{l}	p^{u}
thickness	d [m]	0	100
water content	θ []	0	0.5
decay time	T [s]	0.04	1.0
resistivity	ρ [Ωm]	0	1000

HESSD

9, 2797–2829, 2012

Hydraulic properties on Borkum from joint MRS/VES inversion

T. Günther and M. Müller-Petke

Table 2. Acquisition parameters: loop sizes, number of pulse moments Q and stacks, maximum pulse q_Q, pulse length τ_p and effective dead time Δt_e (see Dlugosch et al., 2011).

Name	Loop size	Q	Stacks	q_Q [As]	τ_p [ms]	Δt_e [ms]
CL2	$49 \times 47\,m^2$	36	16	6.90	40	42
P05	$50 \times 50\,m^2$	36	16	6.86	40	41
OD33	$50 \times 50\,m^2$	44	16	6.70	40	41
SKD	$25 \times 25\,m^2$	46	32	3.42	10	23

HESSD
9, 2797–2829, 2012

Hydraulic properties on Borkum from joint MRS/VES inversion

T. Günther and M. Müller-Petke

HESSD
9, 2797–2829, 2012

Hydraulic properties on Borkum from joint MRS/VES inversion

T. Günther and M. Müller-Petke

Table 3. Retrieved hydraulic parameters for sounding SKD.

	Primary parameters			Secondary parameters	
z [m]	ρ [Ωm]	$\theta = \Phi$	T_2^* [ms]	K [m s^{-1}]	TDS [g l^{-1}]
0–3	10.5	31%	166	4*e*-5	5.8
3–7	1.6	30%	215	7*e*-5	39
7–11	3.6	38%	41	3*e*-6	
11–29	17.6	32%	161	4*e*-5	3.3
29–∞	2.1	27%	489	(3*e*4-4)	31

Table 4. Relative uncertainty of all primary and secondary parameters from sounding SKD.

z [m]	$\delta\rho/\rho$	$\delta\Phi/\Phi$	$\delta T_2^*/T_2^*$	$\delta K/K$	δTDS/TDS
0–3	0.12	0.08	0.10	0.28	0.21
3–7	0.25	0.08	0.11	0.30	0.35
7–11	0.32	0.20	0.18	0.57	0.57
11–29	0.17	0.06	0.07	0.20	0.24
29–∞	0.25	0.17	0.28	0.73	0.46

HESSD

9, 2797–2829, 2012

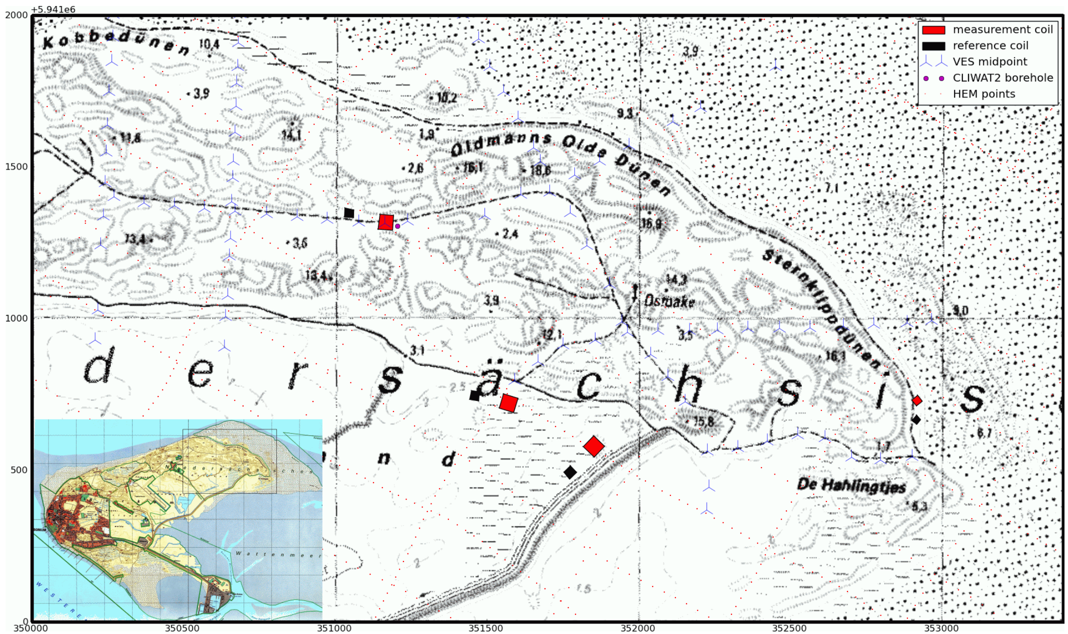

Fig. 1. Measuring area in the east of Borkum and location of MRS measurement (red) and reference (black) coils, VES midpoints (blue tri-stars), the CLIWAT 2 borehole (magenta) and HEM soundings (red dots) in the east dunes of Borkum.

HESSD

9, 2797–2829, 2012

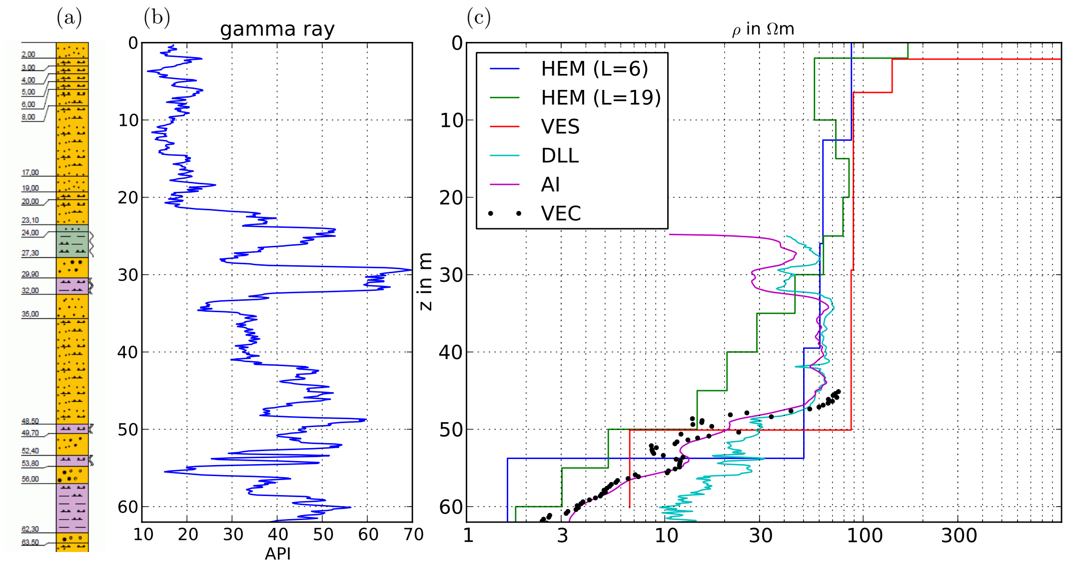

Fig. 2. Lithology **(a)**, gamma ray **(b)** and resistivity information **(c)** at the CLIWAT 2 borehole: 6- and 19-layer HEM solution, VES model, dual laterolog, induction log and vertical electric chain.

HESSD
9, 2797–2829, 2012

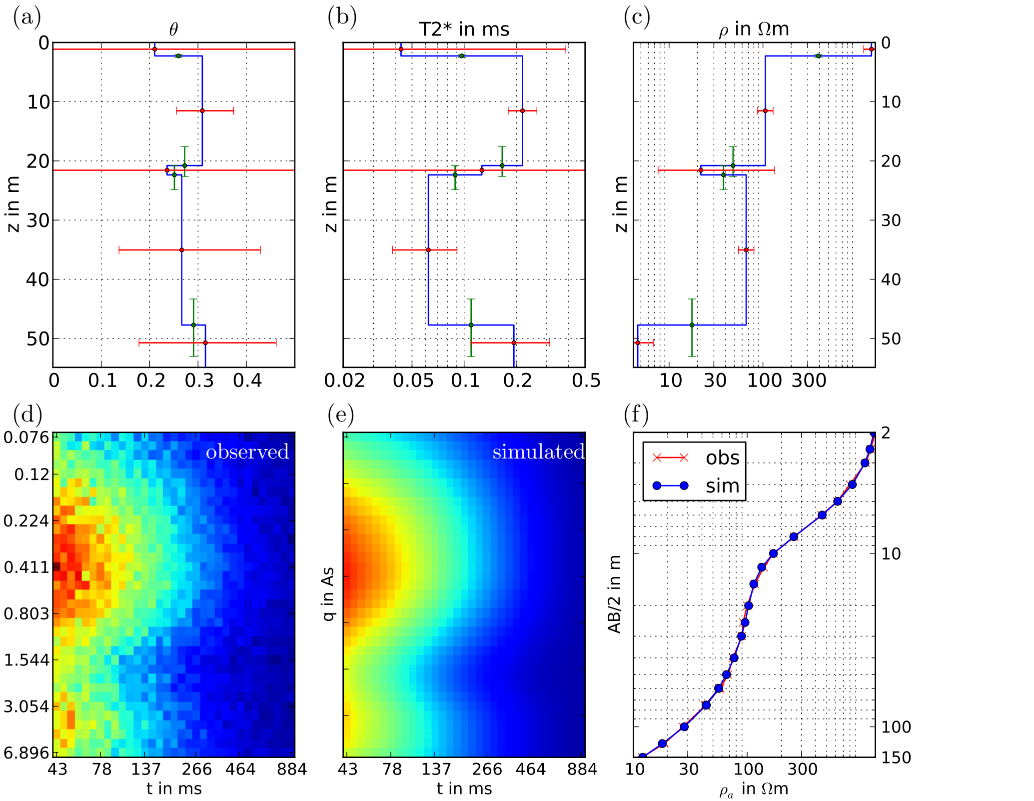

Fig. 3. Joint inversion result of the MRS and VES soundings at the CLIWAT 2 borehole: water content **(a)** decay time **(b)** and resistivity **(c)** as a function of depth including uncertainty, MRS data cube observed **(d)** and simulated **(e)**, and measured/modelled apparent resistivity **(f)**.

HESSD
9, 2797–2829, 2012

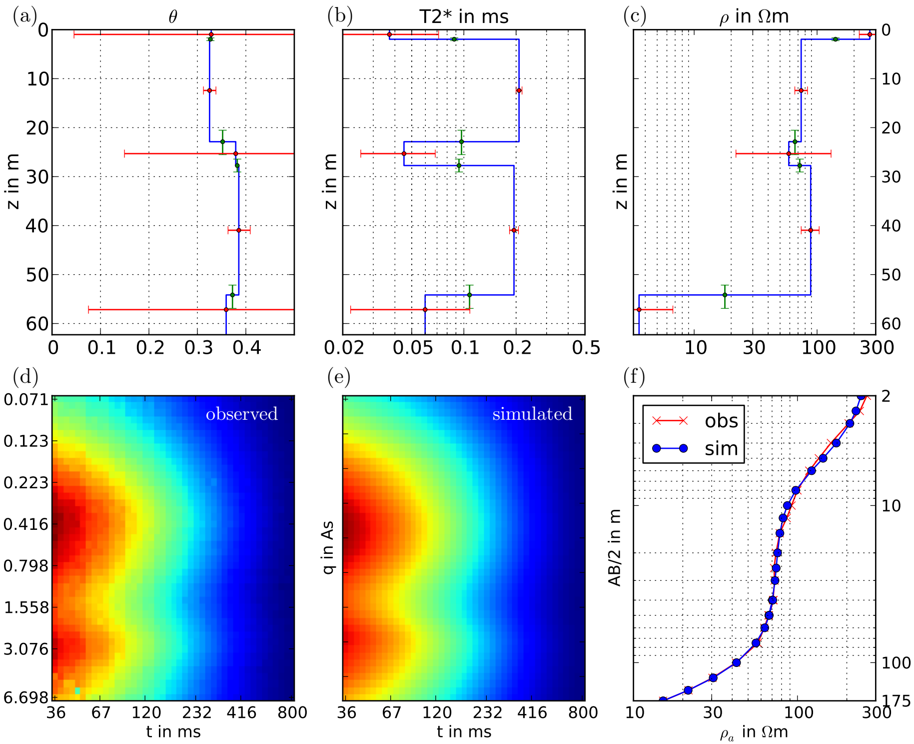

Fig. 4. Joint inversion result (subplots as in Fig. 3) of the MRS and VES soundings for the location OD33.

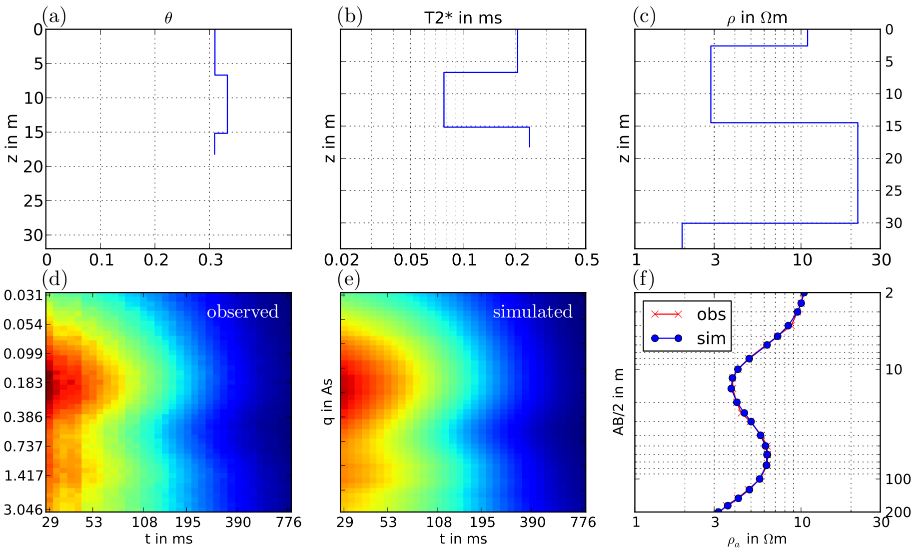

Fig. 5. Result of independent inversions (subplots as in Fig. 3) of the MRS and VES soundings for the location SKD using 3 and 4 layers, respectively.

HESSD
9, 2797–2829, 2012

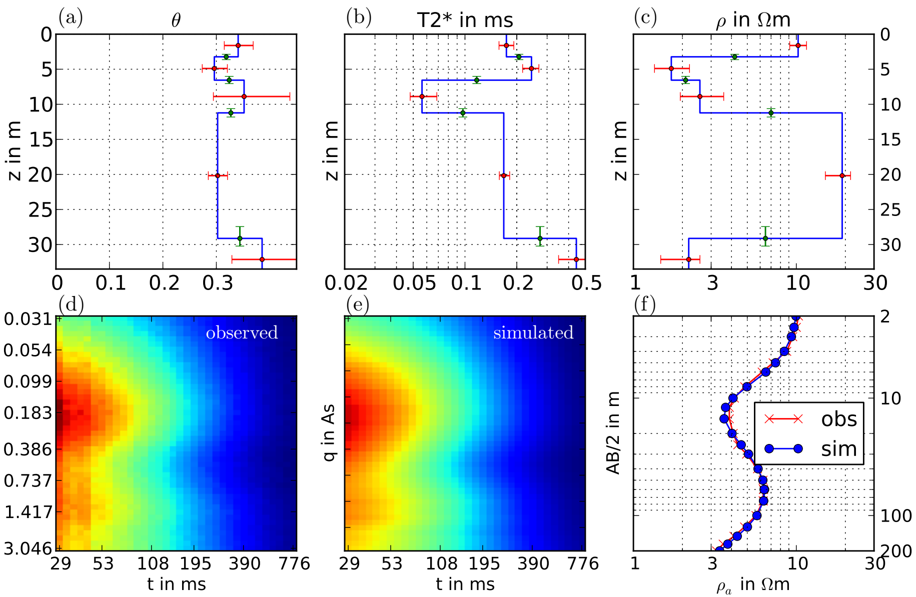

Fig. 6. Joint inversion result (subplots as in Fig. 3) of the MRS and VES soundings for the location SKD.

HESSD
9, 2797–2829, 2012